Heat Mass Transfer (2010) 46:757–768
DOI 10.1007/s00231-010-0622-6

ORIGINAL

Double-diffusive natural convection in inclined finned triangular porous enclosures in the presence of heat generation/absorption effects

Ali J. Chamkha · M. A. Mansour · Sameh E. Ahmed

Received: 24 October 2009 / Accepted: 27 May 2010 / Published online: 11 June 2010

Abstract The problem of double-diffusive convection in inclined finned triangular porous enclosures for various thermal and concentration boundary conditions and in the presence of heat source or sink was studied. The finite difference method was employed to solve the dimensionless governing equations of the problem. The effects of the governing parameters, namely the dimensionless time parameter, the inclination angle, Darcy number, heat generation/absorption parameter, the buoyancy parameter and the Rayleigh number on the streamlines, temperature and concentration contours as well as selected velocity component in the x-direction, local and average Nusselt numbers and local and average Sherwood number at the heated and concentrated wall for various values of the aspect ratio and the position of the fin were considered. The present results are validated by favorable comparisons with previously published results. All the results of the problem were presented in graphical and tabular forms and discussed.

List of symbols

A	Enclosure aspect ratio
c	Dimensionless fin position
C	Dimensional concentration
c_p	Specific heat of the fluid
Da	Darcy number
g	Gravitational acceleration
Gr	Grashof number
h	Dimensionless height of the fin
H	Height of the triangular enclosure
k	Permeability of porous medium
L	Length of the bottom wall of the triangular enclosure
Le	Lewis number
N	Buoyancy parameter
Nu	Nusselt number
Pr	Prandtl number
Q_0	Heat generation/absorption coefficient
Ra	Rayleigh number
Sh	Sherwood number
t	Time
T	Dimensional temperature
u, v	Dimensional velocity components
U, V	Dimensionless velocity components
x, y	Dimensional coordinates
X, Y	Dimensionless coordinates

Greek symbols

α	Effective thermal diffusivity of the porous medium
β_T	Thermal expansion coefficient
β_c	Compositional expansion coefficient
δ	Dimensionless heat generation/absorption parameter
υ	Kinematic viscosity
ϕ	Dimensionless concentration
θ	Dimensionless temperature
ψ	Dimensionless stream function

Subscripts

c	Cold
h	Hot

A. J. Chamkha (✉)
Manufacturing Engineering Department, The Public Authority for Applied Education and Training, 70654 Shuweikh, Kuwait
e-mail: achamkha@yahoo.com

M. A. Mansour
Department of Mathematics, Assuit University, Assuit, Egypt

S. E. Ahmed
Department of Mathematics, South Valley University, Qena, Egypt
e-mail: sameh_sci_math@yahoo.com

1 Introduction

Double-diffusive natural convection in porous media is mainly motivated by its importance in many natural and industrial problems. These include the disposal of waste material, ground water contamination, chemical transport in packed-bed reactors, grain-storage installations, food processing, and drying process, the transport of a contaminant in saturated soil, the migration of moisture in fibrous insulation, etc. Goyeau et al. [1] studied double-diffusive natural convection using Darcy–Brinkman formulation in a porous cavity with impermeable boundaries, horizontal temperature and concentration differences. Bourich et al. [2] studied double diffusive natural convection in a square porous cavity submitted to cross gradients of heat and solute concentration numerically. Bahloul et al. [3] investigated double diffusive convection in a long vertical cavity heated from below and imposed concentration gradient from the sides both analytically and numerically. Double-diffusive steady natural convection in a vertical stack of square enclosures, with heat and mass diffusive walls, was studied numerically by Costa [4]. Gobin et al. [5] focused on the simulation of double-diffusive convective flows in a binary fluid, confined in a vertical enclosure, divided into two vertical layers, one porous and the other fluid. The combined heat and mass transfer rates for natural convection driven by the temperature and concentration gradients in a cavity containing fluid and porous layers was studied by Singh et al. [6] and they showed that the degree of penetration of the fluid into porous region strongly depended upon the Darcy, thermal and solutal Rayleigh number.

Lam et al. [7] examined the natural convection in right triangular, trapezoidal and rectangular enclosures by experimental and numerical methods. Tabbarrok and Lin [8] analyzed natural convection in various geometries by the finite-element method. Karyakin et al. [9] studied laminar natural convection inside isosceles triangular enclosures. Salmun [10, 11] investigated the stability of a single cell steady-state solution in triangular enclosure and with aspect ratio of the enclosure ranging from 0.1 to 1. Lei and Patterson [12] studied unsteady natural convection in a triangular enclosure induced by surface cooling. Holtzmann et al. [13] considered laminar natural convection in isosceles triangular enclosures heated from below and symmetrically cooled from above. Kent et al. [14] considered laminar natural convection in right triangular enclosures with various aspect ratios. On the other hand, natural convection heat transfer induced by internal heat generation has recently received considerable attention because of numerous applications in geophysics and energy-related engineering problems. Such applications include heat removal from nuclear fuel debris, under ground disposal of radioactive waste materials, storage of food stuff, and exothermic chemical reactions in packed-bed reactor (see, for instance, [15–17]).

The phenomenon of heat transfer in cavities is as varied as the geometry and orientation of the enclosure. So, it can be classified as: (1) vertical and inclined cavities heated from the side and (2) horizontal enclosures heated from below. In cavities heated from the side, the problem of natural convection in square cavities heated differentially with adiabatic top and bottom walls has become the classical research problem extensively studied by experimental, analytical and numerical methods to get a better understanding of the governing processes [18–20]. In other geometries and orientations, natural convection in rectangular cavities for various aspect ratios also has been studied extensively; for example, Ozoe et al. [21, 22] dealt with the problem of natural convection in inclined rectangular channels heated on one side and cooled on the opposing side. Their results indicated that as the angle of inclination increased a minimum and then a maximum heat transfer occurred, also, they found out that the angle of inclination was a strong function of the aspect ratio and a weak function of the Rayleigh number. Later, Rahman and Sharif [23] studied the laminar natural convection in differentially heated inclined rectangular enclosures of aspect ratios from 0.25 to 4. Chamkha and Al-Naser [24] considered laminar double-diffusive convective flow of a binary gas mixture in an inclined rectangular enclosure filled with an uniform porous medium. Chamkha and Al-Mudhaf [25] studied double-diffusive natural convection in inclined porous cavities with various aspect ratios and temperature-dependent heat source or sink.

In all of these studies, the authors considered the flows inside rectangular enclosures due simplicity of solutions for the rectangular enclosures. But natural convection in non-rectangular enclosures such as triangular enclosures has received little attention. Tzeng et al. [26] studied natural convection in a roof of triangular enclosures. The problem of natural convection in porous triangular enclosures with the effects of thin fin was studied by Varol et al. [27]. They studied the effects of the problem parameters namely Rayleigh number, various fin lengths and various values of aspect ratio on the fluid motion and heat transfer characteristics but did not study the case of combined heat and mass transfer, the case of various boundary conditions and the case of possible presence of a heat source or sink. Therefore, the main objective of this paper is to study the effects of heat generation/absorption on double-diffusive convection inside an inclined porous triangular enclosure in the presence of a thin fin attached to the bottom wall. A numerical solution based on the finite-difference method is employed to solve the governing equations of the problem. Some graphical and tabular results are presented to illustrate the different influences of the physical parameters on the fluid motion, heat and mass characteristics. The present

study represents generalization of the problem reported for Varol et al. [27] by including heat generation/absorption effect and mass transfer with different boundary conditions.

2 Mathematical model

Consider unsteady, laminar, double-diffusive natural convection flow inside an inclined porous triangular cavity with the effects of thin fin, various thermal and concentration boundary conditions and in the presence of a heat source or sink. In the present problem, the following assumptions have been made:

1. In the triangular cavity, the bottom wall is non-uniformly heated and concentrated, the inclined wall is cooled and have no mass. In any case, the left wall is assumed to be adiabatic and impermeable to mass transfer.
2. An adiabatic and impermeable to mass thin solid fin is considered as a control parameter for fluid flow and heat and mass transfer.
3. Properties of the fluid are isotropic and homogeneous everywhere.
4. A temperature-dependent source/sink of heat generation/absorption in the flow region with constant volumetric rate Q_0 is considered.
5. The viscous dissipation and radiation heating effects are neglected.
6. The density is assumed to be a linear function of temperature and concentration [$\rho = \rho_0\,(1 - \beta_{\mathrm{T}}\,(T - T_c) - \beta_{\mathrm{c}}\,(C - C_c))$].

The geometry and the Cartesian coordinate system are schematically shown in Fig. 1. Under the above assumptions, the governing equations for the problem in general form (after eliminating the pressure gradient terms) can be written as:

$$\nabla^2\psi = -\Omega, \tag{1}$$

$$\Gamma_{S1}\frac{\partial S}{\partial \tau} + \Gamma_{S2}\left(U\frac{\partial S}{\partial X} + V\frac{\partial S}{\partial Y}\right) = \Gamma_{S3}\nabla^2 S + \Phi_S, \tag{2}$$

where S stands for Ω or θ or ϕ and the expressions Γ_{S1}, Γ_{S2}, Γ_{S3} and Φ_S are listed in the following table.

	Ω	θ	ϕ
Γ_{S1}	$1/\varepsilon$	σ	ε
Γ_{S2}	$1/\varepsilon^2$	1.0	1.0
Γ_{S3}	$Pr\,/\varepsilon$	1.0	$1/Le$
Φ_S	$RaPr\left(\frac{\partial\theta}{\partial X} + N\frac{\partial\phi}{\partial X}\right)\cos(\alpha)$ $- RaPr\left(\frac{\partial\theta}{\partial Y} + N\frac{\partial\phi}{\partial Y}\right)\sin(\alpha) - \frac{Pr}{Da}\Omega$	$\delta\theta$	0.0

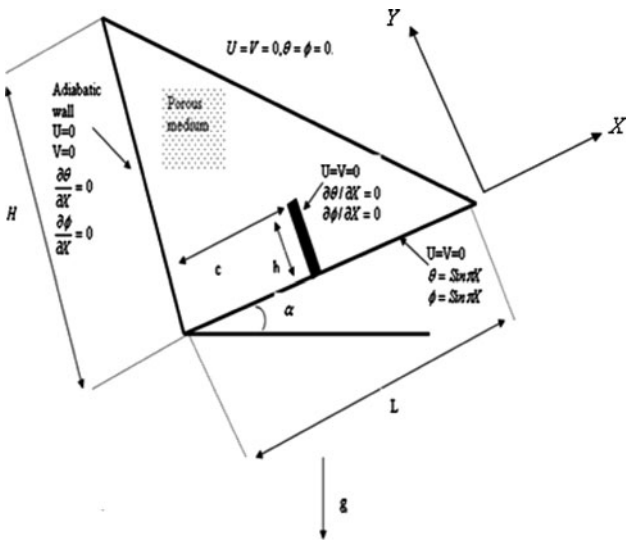

Fig. 1 Physical model of the problem

In the above equations, the following dimensionless variables are employed:

$$X = \frac{x}{L},\ Y = \frac{y}{L},\ \tau = \frac{\alpha t}{L^2},\ \theta = \frac{T - T_r}{T_h - T_r},\ \phi = \frac{C - C_r}{C_h - C_r},$$

$$\Omega = \frac{\zeta L^2}{\alpha},\ \psi = \frac{\Psi}{\alpha},\ u = \frac{\partial\Psi}{\partial y},\ v = -\frac{\partial\Psi}{\partial x},$$

$$\zeta = -\left(\frac{\partial^2\Psi}{\partial x^2} + \frac{\partial^2\Psi}{\partial y^2}\right),$$

$$N = \frac{\beta_{\mathrm{C}}(C_h - C_c)}{\beta_{\mathrm{T}}(T_h - T_c)},\ Le = \frac{\alpha}{D},\ \delta = \frac{Q_0 L^2}{\rho c_p \alpha}$$

$$Ra = \frac{g\beta_{\mathrm{T}}L^3(T_h - T_c)}{\upsilon\alpha},\ \sigma = \frac{\varepsilon\rho c_p + (1-\varepsilon)\rho_s c_s}{\rho c_p}, \tag{3}$$

where all the parameters appearing in the above equations are given in the list of symbols.

The appropriate boundary conditions for the present problem are

$$X = 0\text{: } U = V = \psi = 0,\ \frac{\partial\theta}{\partial X} = 0,\ \frac{\partial\phi}{\partial X} = 0,\ 0 < Y < H,$$
$$Y = 0\text{: } U = V = \psi = 0,\ \theta = \sin(\pi X),\ \phi = \sin(\pi X)$$
$$0 < X < L,$$
$$Y = H - AX,\ U = V = \psi = 0,\ \theta = \phi = 0. \tag{4}$$

On the fin, we have

$$U = V = \psi = 0,\ \frac{\partial\theta}{\partial X} = 0,\ \frac{\partial\phi}{\partial X} = 0, \tag{5}$$

where $A = H/L$ is the enclosure aspect ratio. The boundary condition imposed on the vorticity is written as

$$\Omega_w = -\frac{\partial^2 \psi_w}{\partial S^2} \tag{6}$$

where the subscript w refers to the wall condition and S indicates the direction normal to the wall surface.

The heat and mass transfer coefficients at the enclosure bottom wall in terms of the local Nusselt and Sherwood numbers are defined by

$$Nu = \left(\frac{-\partial\theta}{\partial Y}\right)_{Y=0}, \quad Sh = \left(\frac{-\partial\phi}{\partial Y}\right)_{Y=0}. \tag{7}$$

In addition, the average Nusselt number and Sherwood number at the enclosure bottom wall are defined as

$$\overline{Nu} = \frac{1}{L}\int_0^L Nu\, dX, \quad \overline{Sh} = \frac{1}{L}\int_0^L Sh\, dX. \tag{8}$$

3 Numerical method and validation of the results

The numerical algorithm used to solve the dimensionless governing equations (1)–(2) with the boundary conditions (3) is based on the finite-difference methodology. Central difference quotients are used to approximate the second derivatives in both the X and Y directions. The obtained discretized equations are then solved using the following algorithm:

(a) Select a suitable grid. A grid 21 × 21 is a good start in many cases.
(b) All dependent variables are initialized to zero.
(c) The new boundary values at $(n + 1)$ are calculated for all walls from the previous values at (n).
(d) The new temperature and the new concentration at $(n + 1)$ are calculated from previous (n) values at all internal grid points.
(e) The vorticity and the stream function are calculated in the same way as in step (d).
(f) The velocity components U and V are calculated at $(n + 1)$ from the values at (n) explicitly for all the internal grid points.
(g) The same procedure is followed by starting with step (c) to obtain the solution at the next time step at $(n + 2)$.
(h) The iteration process is terminated if ($\tau \geq$ maxtime) or the following condition satisfies:

$$\sum \left|\chi_{\text{new}}^{n+1} - \chi_{\text{old}}^{n+1}\right| \leq 10^{-5} \tag{9}$$

(i) The Nusselt and Sherwood numbers at the bottom wall are then calculated.
(j) The average Nusselt and average Sherwood numbers at the bottom wall are calculated.

Table 1 Comparison of present results for $\overline{Nu}$ and $\overline{Sh}$ with those of Chamkha and Al-Mudhaf [25] for $Da = 10^{-5}$, $Le = 10.0$, $N = 10$, $Ra = 10^5$ and $\alpha = 0$

	Chamkha and Al-Muhaf [25]		Present results	
α	$\overline{Nu}$	$\overline{Sh}$	$\overline{Nu}$	$\overline{Sh}$
0	1.04196	3.17265	1.049510	3.204658
$\pi/6$	1.05382	3.37160	1.061690	3.413571
$\pi/4$	1.05105	3.25365	1.058802	3.293851
$\pi/3$	1.04190	2.99411	1.049381	3.024590

where χ is the general dependent variable which can stands for θ, ϕ, Ω or ψ and n denotes the iteration step. In order to choose the size of the grid, accuracy tests using finite difference method for mesh sensitivity analysis were performed using four sets of grid: 31 × 31, 61 × 61, 76 × 76 and 101 × 101 as shown in Table 2. Reasonably good agreement was found between 61 × 61 and 101 × 101and therefore, the grid used in this problem was 61 × 61 with a time step of 10^{-4}. In most results to be reported below, the porosity of the porous medium was taken to be 0.6. This method was found to be suitable and gave results that are very close to the numerical results obtained by Chamkha and Al-Mudhaf [25] and Varol et al. [27]. From Figs. 2, 3 and Table 1, we can observe an excellent agreement between our results and the results obtained by Chamkha and Al-Mudhaf [25] and Varol et al. [27]. This favorable comparison lends confidence in the numerical results to be reported subsequently.

4 Results and discussion

In this section, numerical computations are carried out and a parametric study is performed to illustrate the influence of the physical parameters on the resulting streamlines, temperature and concentration contours as well as the horizontal velocity component at the enclosure mid-section, Nusselt and Sherwood numbers at the bottom wall of the enclosure. The results of this parametric study are shown in Figs. 2, 3, 4, 5, 6, 7, 8, 9, 10, 11, 12, 13, 14, 15, 16 and Tables 2, 3, 4, 5, 6, 7. In all of the obtained results, we fixed the length of the fin at the value of 0.3.

Table 3 shows the maximum values of the stream function $\psi_{\max}$ and the minimum values of stream function $\psi_{\min}$ for different values of the dimensionless time parameter τ. It is clear that the absolute values of the stream function decrease transiently as the values of the dimensionless time parameter τ increases until it takes fixed values in the steady state case.

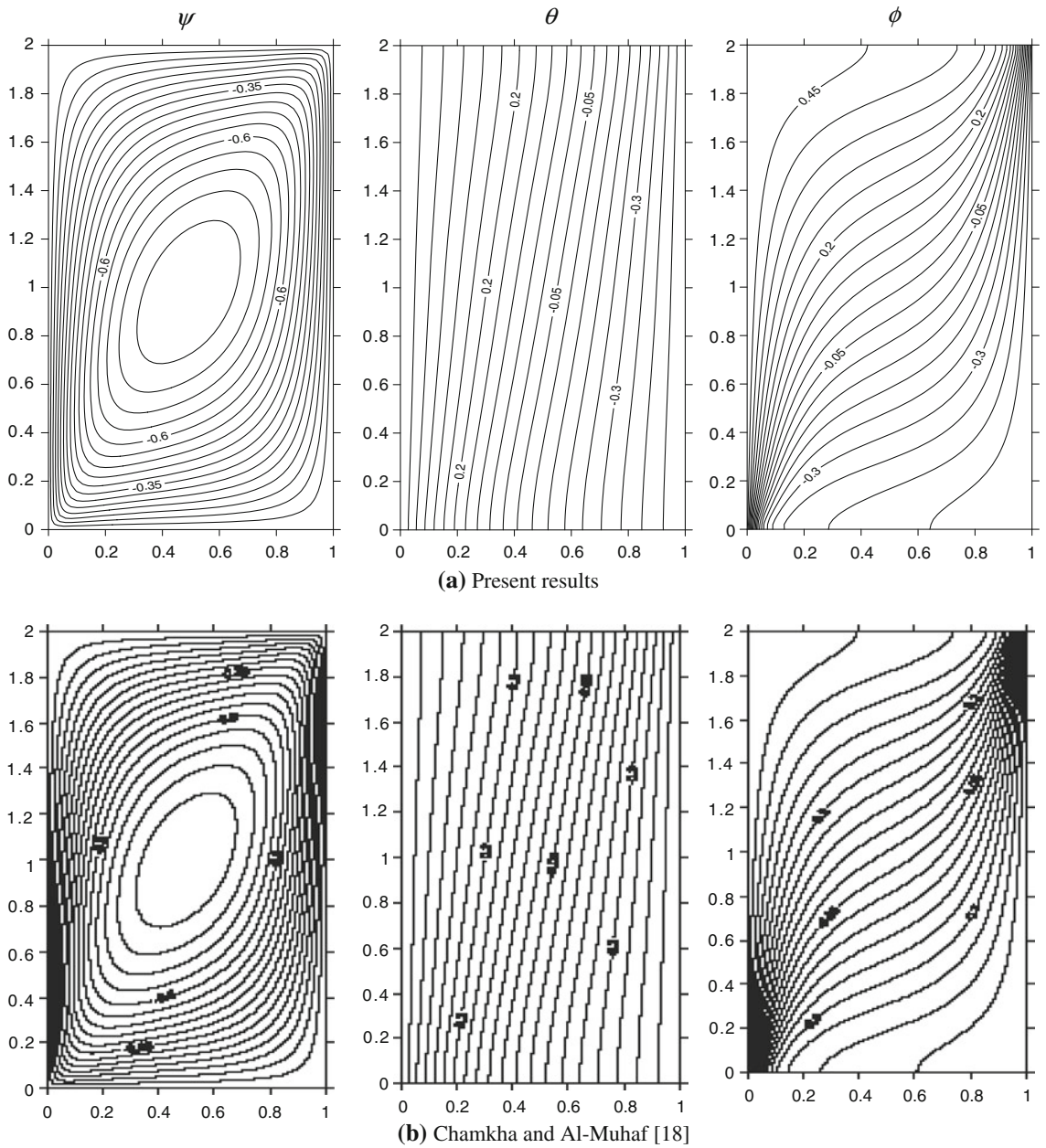

Fig. 2 Comparison of present results with those of Chamkha and Al-Mudhaf [25] for $Da = 10^{-5}$, $Le = 10.0$, $N = 10$, $Ra = 10^5$ and $\alpha = 0$

Figure 4 shows that the streamlines, temperature and concentration contours affected by the inclination angle α (0, $\pi/6$, $\pi/4$, $\pi/2$) of the enclosure. In this case, the aspect ratio of the triangular cavity and the position of the fin were fixed at the values $A = 1.0$ and $X = 0.5$, respectively. When $\alpha = 0$, the fluid moves from the bottom wall to the top corner forming two anti-clockwise and clockwise circular cells before and after the position of the fin, respectively. Also, the contour lines $\psi = -0.015$ and $\psi = -0.005$ start to get pushed towards the top corner of the triangular enclosure. Tilting the triangular enclosure by $\pi/6$, increases the number of the positive contour lines which occur before the position of the fin and these lines tend to stretch along the vertical wall until they become stretched vertically. Moreover, the rate of the fluid motion after the position of the fin decreases when $\alpha = \pi/6$, so we can observe a small number of the counter lines after the position of the fin and a single cell beside the bottom right corner of the triangular enclosure. However, further tilting of the cavity yields an increase in the fluid motion, so when the inclination angle of the enclosure takes the value of $\pi/4$, the rate of the fluid flow increases until the stream function takes the largest value when $\alpha = \pi/2$ ($\psi_{max} = 0.125$). Regarding to the temperature contours, all of the constant

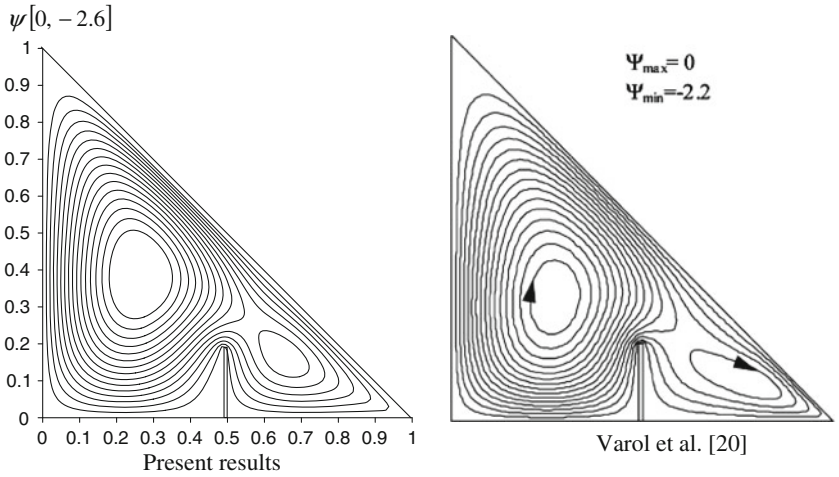

Fig. 3 Comparison of present results with those of Varol et al. [27] problem for $Ra = 10^3$ and $\alpha = 0$

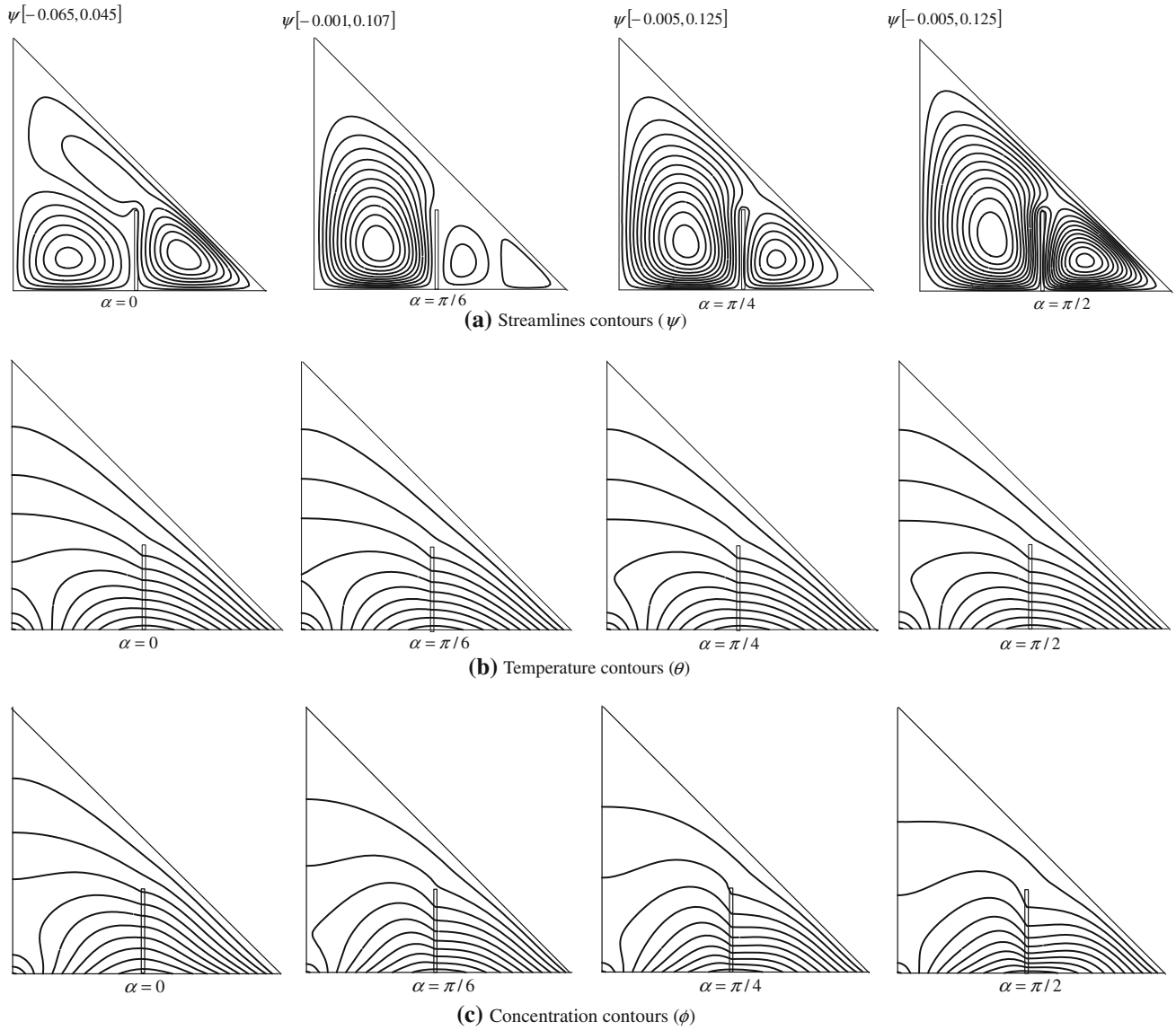

Fig. 4 Streamlines, temperature and concentration contours for various values of the inclination angle α for $Da = 10^{-5}$, $Le = 10.0$, $N = 10$, $Ra = 10^5$ and $\delta = 5.0$

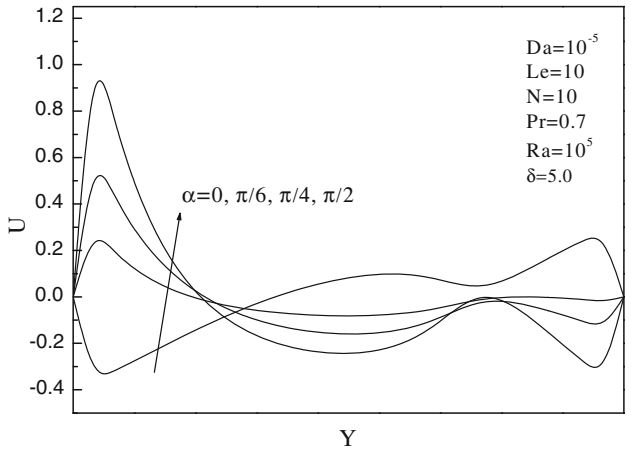

Fig. 5 Effect of the inclination angle α on horizontal velocity component at the enclosure mid-section

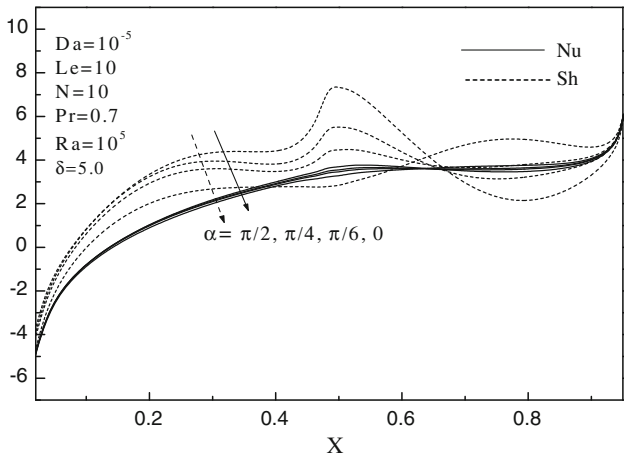

Fig. 6 Effect of the inclination angle α on the Nusselt and Sherwood numbers at the enclosure bottom wall

temperature lines start at different places from the horizontal wall and then these lines get divided such that the temperature lines $\theta \leq 0.35$ occur in two regions, one of them at the left bottom corner in symmetrical form and the other occurs at top half of the triangular enclosure. The remaining constant temperature lines $\theta \geq 0.4$ start from different places before the fin and vanish after some distance from the fin. In addition, tilting the triangular enclosure by $\pi/4$ decreases the number of the temperature lines which arise at the bottom left corner to include all lines $\theta \leq 0.3$ and the isotherm contour line $\theta = 0.35$ starts to get pushed towards the vertical wall of the cavity. Increasing the value of the inclination angle leads to an increase in the area which covered by the temperature lines. From Fig. 4c, we can observe the behaviors of the iso-concentration lines for different values of the inclination angle α. These behaviors are similar to the behaviors of the constant temperature lines, the concentration

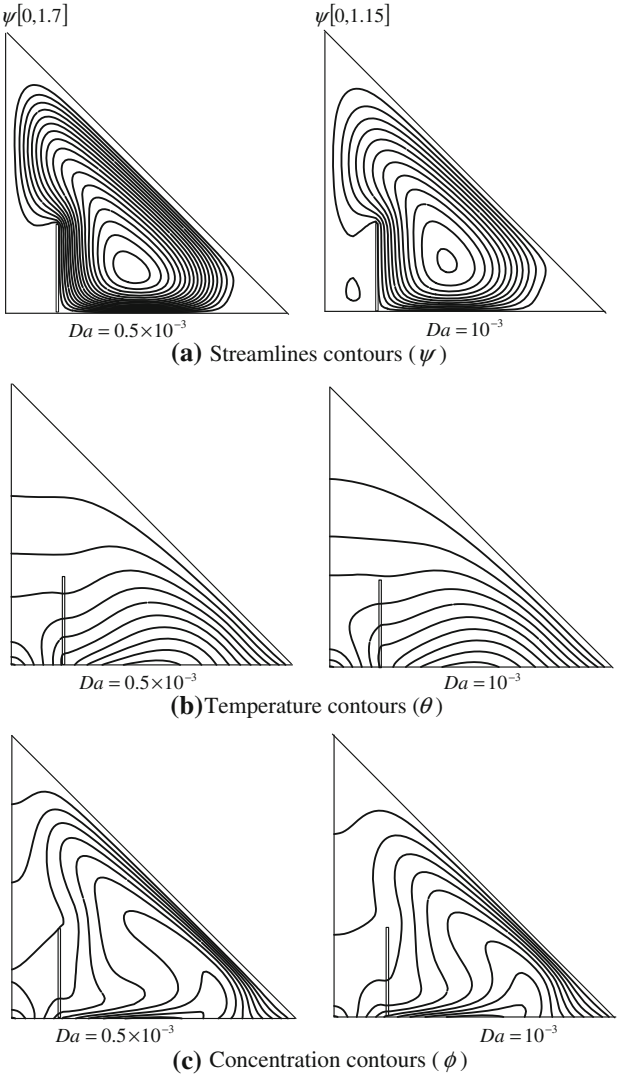

Fig. 7 Streamlines, temperature and concentration contours for various values of the Darcy number Da for $Le = 10.0$, $N = 5.0$, $Ra = 10^4$, $\alpha = \pi/4$ and $\delta = 5.0$

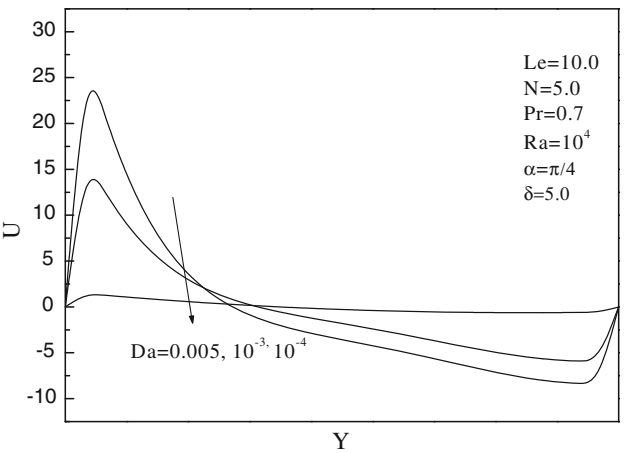

Fig. 8 Effect of the Darcy number Da on the horizontal velocity component at the enclosure mid-section

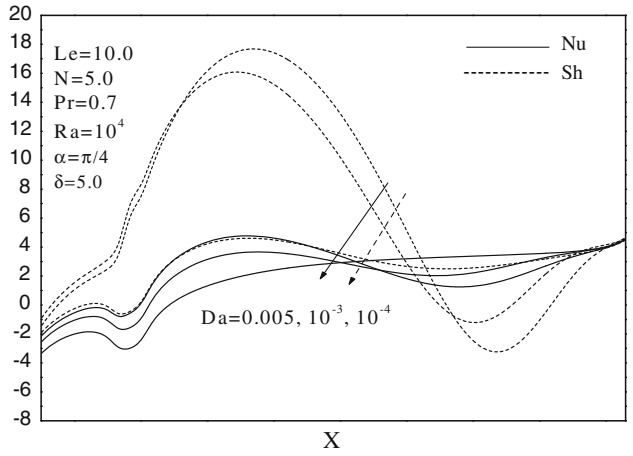

Fig. 9 Effect of the Darcy number *Da* on the Nusselt and Sherwood numbers at the enclosure bottom wall

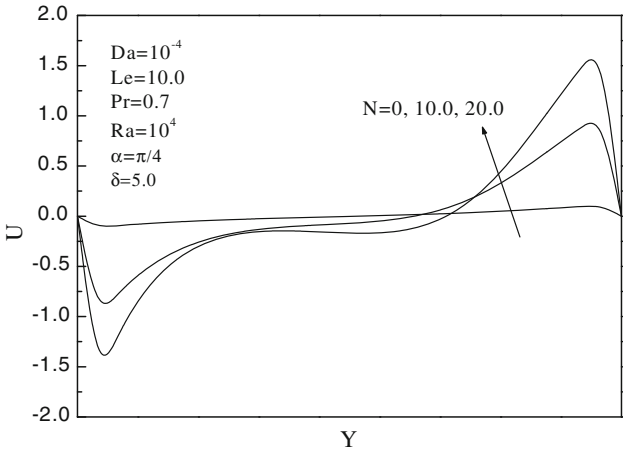

Fig. 11 Effect of the buoyancy parameter *N* on the horizontal velocity component at the enclosure mid-section

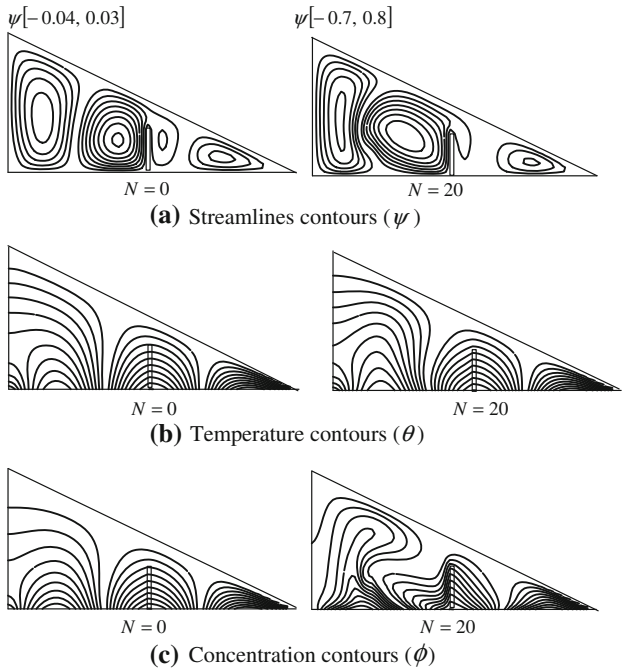

Fig. 10 Streamlines, temperature and concentration contours for various values of the buoyancy parameter *N* for $Da = 10^{-4}$, $Le = 10.0$, $Ra = 10^4$, $\alpha = \pi/4$ and $\delta = 5.0$

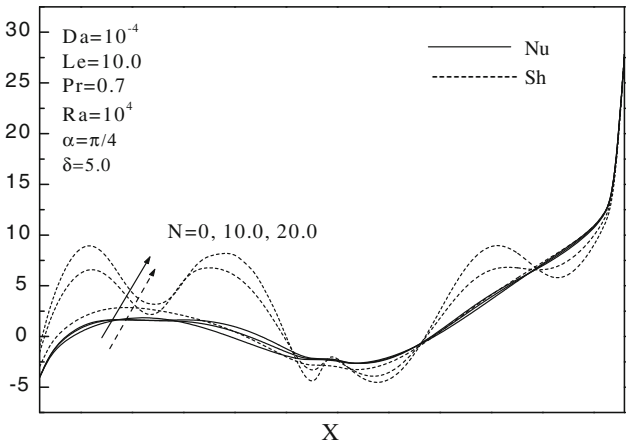

Fig. 12 Effect of the buoyancy parameter *N* on the Nusselt and Sherwood numbers at the enclosure bottom wall

contours $\phi \leq 0.3$ for the non-inclined cavity ($\alpha = 0$) occur at two places, one of them at the left bottom corner in symmetrical form and the other occur at the top half of the triangular cavity and the other lines start from different places before the position of the fin and vanish after some distance after the position of the fin. Increasing the value of the inclination angle of the triangle results in a decrease in the number of the iso-concentration contour lines which occur in the bottom left corner to become all uniform lines of $\phi \leq 0.2$ when $\alpha = \pi/6$ and all uniform lines of $\phi \leq 0.15$ when $\alpha = \pi/4$ and $\alpha = \pi/2$.

With the help of Figs. 5 and 6, we can observe the effect of the inclination angle α on the horizontal velocity component at the triangular enclosure mid-section and the effect of the inclination angle α on the Nusselt and Sherwood numbers at the enclosure bottom wall, respectively. It is clear that, increasing the value of the inclination angle α leads to not only increase the horizontal velocity component but also to increase the Nusselt and Sherwood numbers. In addition, the effect of the inclination angle α on the average Nusselt and Sherwood numbers at the enclosure bottom wall can be observed from Table 4. It is predicted that increasing the value of the inclination angle α leads to increases in both of the average Nusselt and Sherwood numbers.

For a fixed value of the inclination angle ($\alpha = \pi/4$), we studied the effect of the porous medium represented by the Darcy number *Da* on the streamlines, constant temperature and concentration line contours as shown in Fig. 7. In this

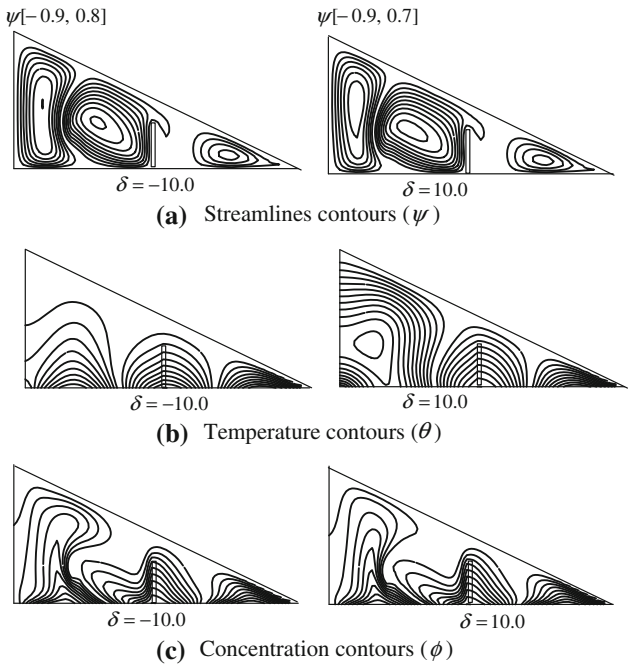

Fig. 13 Streamlines, temperature and concentration contours for various values of the heat generation/absorption parameter δ for $Da = 10^{-3}$, $Le = 10.0$, $N = 5.0$, $Ra = 5 \times 10^3$ and $\alpha = \pi/4$

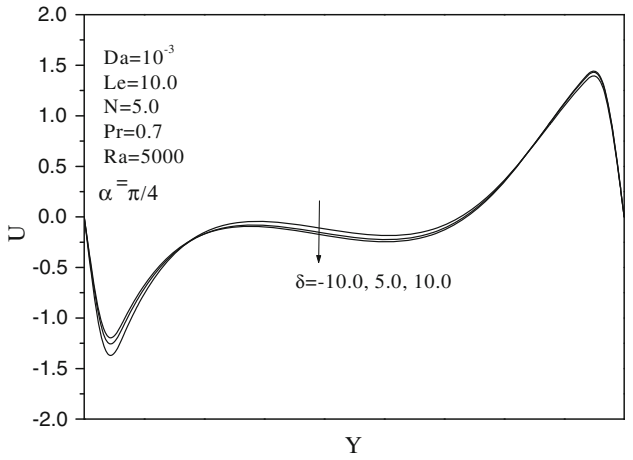

Fig. 14 Effect of the heat generation/absorption parameter δ on the horizontal velocity component at the enclosure mid-section

case, we changed the position of the fin to become at $X = 0.2$. It is found that, there is a single anti-clockwise cell formed inside the triangular enclosure with $\psi_{\max} = 1.7$ when $Da = 0.5 \times 10^{-3}$ and there are no lines inside the region ($0 \le X \le 0.2$, $0 \le Y \le 0.3$). When $Da = 10^{-3}$, the largest value of the stream function become $\psi_{\max} = 1.15$ and there is small line occurring inside the region ($0 \le X \le 0.2$, $0 \le Y \le 0.3$). In addition, the region which can be covered by the temperature contour lines in the case when $Da = 10^{-3}$ is bigger than the region when

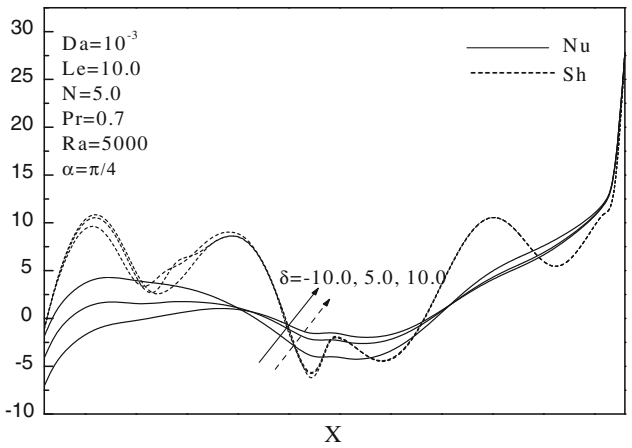

Fig. 15 Effect of the heat generation/absorption parameter δ on the Nusselt and Sherwood numbers at the enclosure bottom wall

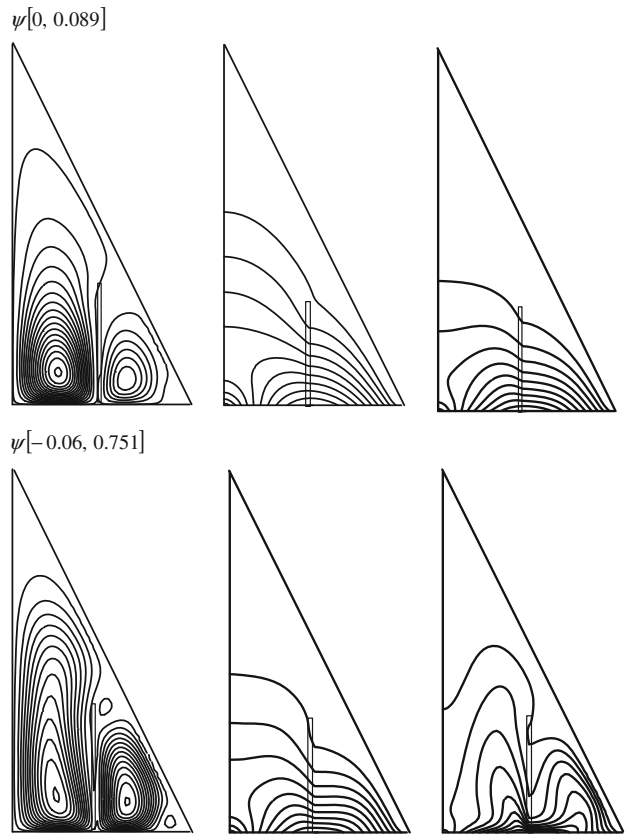

Fig. 16 Contours of streamlines (*left*), temperature (*right*) and concentration (*left*) at $Ra = 10^3$, 10^4. (Increasing from *top* towards *bottom*)

$Da = 0.5 \times 10^{-3}$. Moreover, the iso-concentration contours have a slight effect by the change in the value of the Darcy number. When the Darcy number decreases, the number of iso-concentration lines which occur at the bottom left corner decreases to become all uniform lines of $\phi \le 0.15$.

Table 2 Accuracy test for $A = 1$, $Da = 10^{-5}$, $Le = 10$, $N = 5$, $Pr = 0.7$, $Ra = 10^5$, $\alpha = \pi/4$, $\delta = 5$

Nodes	ψ_{max}	ψ_{min}
31 × 31	0.1219569	−0.0032416
61 × 61	0.1277552	−0.0016309
76 × 76	0.1272008	−0.0012974
101 × 101	0.1298482	−0.0010037

Table 3 Effect of dimensionless time parameter τon the maximum and minimum values of stream function when $A = 1$, $Da = 10^{-5}$, $Le = 10$, $N = 5$, $Pr = 0.7$, $Ra = 10^5$, $\alpha = \pi/4$, $\delta = 5$

τ	ψ_{max}	ψ_{min}
0.2	0.1446745	−0.0021376
0.3	0.1406185	−0.0020412
0.5	0.13337	−0.0018117
Steady state	0.1277552	−0.0016309

Table 4 Effect of the inclination angle α on the average Nusselt and Sherwood numbers at the enclosure bottom wall

α	$\overline{Nu}$	$\overline{Sh}$
0	2.4362570	2.9666220
$\pi/6$	2.4690450	3.2398980
$\pi/4$	2.4818450	3.3861440
$\pi/2$	2.4945430	3.5659070

Table 5 Effect of the Darcy number *Da* on average Nusselt and Sherwood numbers at the enclosure bottom wall

Da	$\overline{Nu}$	$\overline{Sh}$
0.5×10^{-3}	2.3162690	6.3426210
10^{-3}	2.0707750	6.0996050
10^{-4}	1.7367570	2.6363770

Table 6 Effect of the buoyancy parameter *N* on the average Nusselt and Sherwood numbers at the enclosure bottom wall

N	$\overline{Nu}$	$\overline{Sh}$
0	2.0407350	2.3534290
10	2.1726400	3.8328010
20	2.2733740	4.4561580

Table 7 Effect of the heat generation/absorption parameter δ on the Nusselt and Sherwood numbers at the enclosure bottom wall

δ	$\overline{Nu}$	$\overline{Sh}$
−10	2.7110150	4.7776000
5	2.3339700	4.8235960
10	1.8301240	4.7696190

In Figs. 8 and 9, the effects of the Darcy number *Da* on the horizontal velocity component at the enclosure mid-section, Nusselt and Sherwood numbers at the bottom wall of the cavity are presented, respectively. It is clear that, increasing the value of the Darcy number leads to increases in the horizontal velocity component and the Nusselt and Sherwood numbers. Table 5 shows the magnitude values of the average Nusselt and Sherwood numbers for various values of the Darcy number. As we expect, the largest value of the Darcy number gives the largest value of the average Nusselt and Sherwood numbers.

The effect of buoyancy parameter *N* on the streamlines, temperature and concentration contours for a fixed value of the inclination angle ($\alpha = \pi/4$) is plotted in Fig. 10. For this case, we decreased the enclosure aspect ratio to $A = 1/3$. It is seen that three clockwise and anti-clockwise circular cells are formed inside the cavity. Two of them are before the position of the fin and the other is after the position of the fin. In the absence of buoyancy force ($N = 0$), there exists a weak motion with $\psi_{min} = -0.04$ and $\psi_{max} = 0.03$ but when the buoyancy parameter take a larger value ($N = 20$), the rate of the fluid motion increases and the maximum and minimum values of the stream function become $\psi_{min} = -0.7$ and $\psi_{max} = 0.8$. In addition, the problem boundary conditions show that the temperature and the concentration of the fluid are slightly affected by the decrease of the enclosure aspect ratio. The ranges of θ and ϕ in this case are $-1.0 \leq \theta \leq 1.0$ and $-1.0 \leq \phi \leq 1.0$, respectively. The positive temperature and concentration lines occur at two regions one of them is at $0 \leq X \leq 1.0$ and the other is at $2.0 < X \leq 3.0$ but the negative temperature and concentration lines arise at the region $1.0 < X \leq 2.0$. When the buoyancy parameter takes the value $N = 20$, the concentration contours cover an area of the triangular enclosure larger than that corresponding to $N = 0$.

Figures 11 and 12 display the effects of buoyancy parameter *N* on the selected horizontal velocity component, Nusselt and Sherwood numbers at the bottom wall of the enclosure, respectively. It is clear that, increasing the value of the buoyancy parameter *N* results in increases in the horizontal velocity component, Nusselt number and Sherwood numbers. Table 6 shows the effect of the buoyancy parameter *N* on the average Nusselt number and the average Sherwood number. As expected, the presence of the buoyancy force increases both of the average Nusselt and Sherwood numbers.

Figure 13 shows the effect of the heat generation/absorption parameter δ on the streamlines, temperature and concentration contours for a fixed value of the inclination angle ($\alpha = \pi/4$) and triangular cavity aspect ratio $A = 1/3$. From this figure, we can observe that the presence of a heat sink ($\delta = -10.0$) tends to accelerate the fluid motion but

the presence of a heat source ($\delta = 10.0$) leads to a deceleration in the fluid motion. In addition, the temperature of the fluid increases by increasing the heat generation/absorption parameter δ and the number of positive line increase to include $\theta = 1.2$ in the case of a heat source. The concentration contours are not affected slightly by the increase in the heat generation/absorption parameter δ except that the concentration lines become more asymptotic in the case of a heat source than in the case of a heat sink.

The effect of the heat generation/absorption parameter δ on the horizontal velocity component at the enclosure midsection as well as the Nusselt and Sherwood numbers at the bottom wall of the enclosure are presented in Figs. 14 and 15, respectively. It is observed that increasing the value of δ leads to a decrease in the horizontal velocity component whereas the Nusselt and Sherwood numbers take the opposite behavior. Table 7 presents the values of the average Nusselt and Sherwood numbers at the enclosure bottom wall for various values of the heat generation/absorption parameter δ. From this table, we observe that the presence of a heat source results in higher Nusselt and Sherwood numbers values than those corresponding to the presence of a heat sink. All these behaviors are presented in Figs. 13, 14, 15 and Table 5 with reference values of $Da = 10^{-3}$, $Le = 10.0$, $N = 5$, $Pr = 0.7$, $Ra = 5 \times 10^3$.

Finally, we generalized our problem by considering another value of the aspect ratio $A = 2.0$. This is clearly found in Fig. 16 which shows the effect of Rayleigh number Ra on the contours of the stream function, isotherms and isoconcentration. From this figure, we observe that the fluid motion becomes more complex and the maximum and minimum values of the stream function change from $\psi_{\max} = 0.089$, $\psi_{\min} = 0$ when $Ra = 10^3$ to the values $\psi_{\max} = 0.751$, $\psi_{\min} = -0.06$ when $Ra = 10^5$. Also, the streamlines follow the geometry of the triangle by forming two clockwise circular cells when $Ra = 10^3$ and four clockwise and anti-clockwise circular cells when $Ra = 10^5$. Regarding the isotherms and isoconcentration contours, they become more asymptotic when Ra increases. The reference case parametric values of these behaviors are $Da = 10^{-3}$, $Le = 10$, $N = 5$, $Pr = 0.7$, $\alpha = \pi/4$, $\delta = 5$.

5 Conclusions

In the present paper, double-diffusive convection in an inclined porous triangular enclosure with the effects of a thin fin placed at the bottom wall, various temperature and concentration boundary conditions in the presence of a heat source or sink was studied. The finite-difference method was employed for the solution of the present problem. Comparisons with previously published work on special cases of the problem were performed and found to be in excellent agreement. Graphical and tabular results for various parametric conditions were presented and discussed. From this investigation, we can draw the following conclusions:

1. In general, the rate of fluid motion, heat and mass characteristics increased by increasing the inclination angle of the triangular enclosure.
2. A faster motion in the cavity was predicted when the Darcy number increased and the average Nusselt and Sherwood numbers took the same behavior.
3. Increasing the buoyancy ratio parameter led to increases in both of the average Nusselt and Sherwood numbers.
4. The presence of a heat sink caused acceleration of the fluid motion but the presence of a heat source caused deceleration in the fluid motion.
5. Increasing the heat generation/absorption parameter caused increases in the Nusselt and Sherwood numbers.

References

1. Goyeau B, Songbe D, Gobin J-P (1996) Numerical study of double- diffusive natural convection in a porous cavity using the Darcy–Brinkman formu-lation. Int J Heat Mass Transfer 39:1363–1378
2. Bourich M, Amahmid A, Hasnaoui M (2004) Double diffusive convection in a porous enclosure submitted to cross gradients of temperature and concentration. Energy Convers Manag 45:1655–1670
3. Bahloul A, Kalla L, Bennacer R, Beji H, Vasseur P (2004) Natural convection in a vertical porous slot heated from below and with horizontal concen-tration gradients. Int J Ther Sci 43:653–663
4. Costa VAF (1997) Double diffusive natural convection in a square enclosure with heat and mass diffusive walls. Int J Heat Mass Transf 40:4061–4071
5. Gobin D, Goyeau B, Neculae AA (2005) Convective heat and solute transfer in partially porous cavities. Int J Heat Mass Transf 48:1898–1908
6. Singh AK, Paul T, Thorpe GR (1999) Natural convection due to heat and mass transfer in a composite system. Heat Mass Transf 35:39–48
7. Lam SW, Gani R, Symons JG (1989) Experimental and numerical studies of natural convection in trapezoidal cavities. ASME J Heat Transf 111:372–377
8. Tabarrok B, Lin RC (1977) Finite element analysis of free convection flows. Int J Heat Mass Transf 20:945–952
9. Karyakin YUE, Sokovishin YUA, Martynenko OG (1988) Transient natural convection in triangular enclosures. Int J Heat Mass Transf 31:1759–1766
10. Salmun H (1995) The stability of a single-cell steady-state solution in a triangular enclosure. Int J Heat Mass Transf 38:363–369
11. Salmun H (1995) Convection patterns in a triangular domain. Int J Heat Mass Transf 38:351–362
12. Lei C, Patterson JC (2005) Unsteady natural convection in a triangular enclosure induced by surface cooling. Int J Heat Fluid Flow 26:307–321

13. Holtzmann GA, Hill RW, Ball KS (2000) Laminar natural convection in isosceles triangular enclosures heated from below and symmetrically cooled from above. ASME J Heat Transf 122:485–491
14. Kent EF, Asmaz E, Ozerbay S (2007) Laminar natural convection in right triangular enclosures. Heat Mass Transf 44:187–200
15. Kakac S, Aung W, Viskanta R (1985) Natural convection—fundamentals and applications. Hemisphere, Washington, DC
16. Chamkha AJ, Al-Naser H (2002) Hydromagnetic double-diffusive convection in a rectangular enclosure with uniform side heat and mass fluxes and opposing temperature and concentration gradients. Int J Therm Sci 41:936–948
17. Grosan T, Revnic C, Pop I, Ingham DB (2009) Magnetic field and internal heat generation effects on the free convection in a rectangular cavity filled with a porous medium. Int J Heat Mass Transf 52:1525–1533
18. Ivey GN (1984) Experiments on transient natural convection in a cavity. J Fluid Mech 144:389–401
19. Ostrach S (1988) Natural convection in enclosures. J Heat Transf 110:1175–1190
20. Paolucci S, Chenoweth DR (1988) Natural convection in shallow enclosures with differentially heated endwalls. J Heat Transf 110:625–634
21. Ozoe H, Sayama H, Churchill S (1974) Natural convection in an inclined square channel. Int J Heat Mass Transf 17:401–406
22. Ozoe H, Sayama H, Churchill S (1975) Natural convection in an inclined rectangular channel at various aspect ratios and angles-experimental measurements. Int J Heat Mass Transf 18:1425–1431
23. Rahman R, Sharif MA (2003) Numerical study of laminar natural convection in inclined rectangular enclosures of various aspect ratios. Numer Heat Transf Part A 44:355–373
24. Chamkha AJ, Al-Naser H (2001) Double-diffusive convection in an inclined porous enclosure with opposing temperature and concentration gradients. Int J Therm Sci 40:227–244
25. Chamkha AJ, Al-Mudhaf A (2008) Double-diffusive natural convection in inclined porous cavities with various aspect ratios and temperature-dependent heat source or sink. Heat Mass Transf 44:679–693
26. Tzeng SC, Liou JH, Jou RY (2005) Numerical simulation-aided parametric analysis of natural convection in a roof of triangular enclosures. Heat Transf Engrg 26:69–79
27. Varol Y, Oztop HF, Varol A (2007) Effects of thin fin on natural convection in porous triangular enclosures. Int J Ther Sci 46:1033–1045